catalysts

Article

Designed Synthesis of PDI/BiOCl-$BiPO_4$ Composited Material for Boosted Photocatalytic Contaminant Degradation

Huaqiang Zhuang [1,*], Fulin Wang [2], Kaiyang Shi [2] and Kai Yang [2,*]

[1] College of Chemical Engineering and Materials Science, Quanzhou Normal University, Quanzhou 362000, China
[2] School of Chemistry and Chemical Engineering, Jiangxi University of Science and Technology, Ganzhou 341000, China
* Correspondence: huaqiangz@163.com (H.Z.); yangkai@jxust.edu.cn (K.Y.)

Abstract: Enhancing the photocatalytic performance for contaminant degradation to accelerate the large-scale application of photocatalysis still is an enduring challenge. Herein, ternary PDI/BiOCl-$BiPO_4$ composited materials with the different contents of PDI were designed and constructed by the multi-step compound method. The tetracycline hydrochloride and rhodamine B were chosen as targeted pollutants to investigate the photocatalytic performance of PDI/BiOCl-$BiPO_4$ composited materials. The structure and component of BiOCl-$BiPO_4$ and PDI/BiOCl-$BiPO_4$ samples were detailedly characterized by a sequence of physical and chemical characterizations. The optimized PDI/BiOCl-$BiPO_4$ sample, namely PDI(5%)/BiOCl-$BiPO_4$, exhibited the excellent photocatalytic activity for tetracycline hydrochloride and rhodamine B degradation. The major active species that were holes (h^+) and superoxide radicals ($\bullet O_2^-$) also can be determined in the photocatalytic degradation process by active species trapping experiments. Furthermore, the photoelectrochemical and fluorescence measurements manifest the crucial role of PDI material. It can reduce the recombination of photo-excited charge carrier and improve the separation and transfer of photo-generated electron-hole pairs, which is beneficial to the photocatalytic reaction process. It is anticipated that our work would provide a counterpart to prepare the high-efficiency composited material in heterogeneous photocatalysis.

Keywords: PDI; BiOCl/$BiPO_4$; photocatalytic; degradation; contaminant

Citation: Zhuang, H.; Wang, F.; Shi, K.; Yang, K. Designed Synthesis of PDI/BiOCl-$BiPO_4$ Composited Material for Boosted Photocatalytic Contaminant Degradation. *Catalysts* **2023**, *13*, 688. https://doi.org/10.3390/catal13040688

Academic Editor: Vincenzo Vaiano

Received: 13 February 2023
Revised: 22 March 2023
Accepted: 30 March 2023
Published: 31 March 2023

1. Introduction

Currently, energy and environmental issues have attracted great attention all over the world. Recent years, the overuse of antibiotic has seriously damaged ecological environment and harmed human health [1–3]. Tetracycline hydrochloride (TCH) is considered as one of the most commonly used antibiotic for the cure of pneumonia, trachoma, and bacterial dysentery [4–6]. Nevertheless, its long-term retention determines the prolong time in the water body or environment, so the elimination of TCH still needs to be addressed immediately [7–10]. Photocatalytic technology is a promising strategy to resolve water pollution problems and provide the green energy demand, attributing to the advantages of non-toxic, cheap, sustainable energy, stable and reusable photocatalysts [11–14]. The degradation of TCH through photocatalytic technology is an idea approach. It can't only utilize the solar energy, but also avoid the secondary pollution. Raja [14] et al. found that the hierarchical $ZnIn_2S_4$/rGO/SnS_2 heterojunction photocatalyst possessed the higher photocatalytic activities for hydrogen evolution and photocatalytic degradation performance towards tetracycline (TC). The enhanced photocatalytic active mainly is attributed to the hexagonal and layer structured material and the synergetic effect of $ZnIn_2S_4$/rGO/SnS_2 heterojunction photocatalyst. Zhi [15] et al. reported that the direct Z-scheme $ZnIn_2S_4$@MoO_3 heterojunction was prepared and evaluated by the degradation of tetracycline hydrochloride under visible light irradiation. The $ZnIn_2S_4$@MoO_3 composited material displayed a high photocatalytic performance, which could degrade 94.5% of TCH with 90 min. The mechanism for degradation of TCH and the possible reaction pathway were also proposed. In addition, the $NiFe_2O_4$/g-C_3N_4 heterostructure was designed and prepared to degrade the tetracycline hydrochloride antibiotic [9]. The optimized $NiFe_2O_4$/g-C_3N_4 sample exhibited high photocatalytic degradation efficiency with 94.5% in 80 min under visible light irradiation. These reports clearly indicate that photocatalytic pollutant degradation is an effective means to resolve the antibiotic contamination, but the photocatalytic systems still exist some deficiencies. Herein, it is necessary to explore some novel or effective photocatalysts.

BiOCl material with a layer structure consists of $[Bi_2O_2]^{2+}$ slab interlaced by double halogen slabs, resulting in the formation of internal static electric fields, which is beneficial to the separation of photo-generated electron-hole pairs. It is the unique structure that urges photogenerated carriers to easily facilitate separation and transfer leading to the enhanced photocatalytic performance [16]. In addition, it has the merits of high chemical stability, corrosion resistance and non-toxicity. So BiOCl is regarded as the excellent photocatalytic substrate. However, there is still need for improving their photocatalytic activity before practical use. Zhuang [17] et al. prepared the BiOCl with oxygen vacancy via a novel strategy to improve the photocatalytic performance. Su [18] et al. studied that reduced graphene oxide nanosheets (RGO) were introduced into 50% BiOCl/BiOI hollow flowerlike microspheres to improve the photocatalytic degradation of rhodamine B under visible light irradiation. These strategies can effectively improve the photocatalytic performance of BiOCl, especial for the composited method.

Recently, $BiPO_4$ has aroused many scholars' attention, because it possesses excellent ultraviolet active, stability, strong oxidation ability, non-toxicity and unique electronic properties. The inherently induced effect of phosphate radical is beneficial to the separation of electron-hole pairs, which is considered to be the reason for enhancing photocatalytic activity compared to TiO_2 [19–21]. It can show the better performance for pollutant degradation than that of P25, and the photocatalytic active of $BiPO_4$ is twice that of TiO_2 for the degradation of methylene blue (MB) due to the inductive effect of phosphate group (PO_4^{3-}) [21]. However, its wide band gap of 3.85 eV and high charge recombination limit the photocatalytic performance [22,23]. Therefore, introducing a suitable semiconductor to reduce the band gap and improve the separation efficiency of photo-generated charge carriers is an effective strategy to enhance the photocatalytic performance. Currently, perylene diimide (PDI)-based photocatalysts with n-type organic semiconductor have been applied in photocatalytic pollutant degradation and water splitting [24,25]. PDI material possesses narrow band gap and suitable conduction band position, which can improve the visible light absorption and photocatalytic activity of semiconductor photocatalyst [26–28]. Zhu [26] et al. reported that the p-Ag_2S/n-PDI self-assembly supramolecular heterojunction was formed via hydrogen bonding and $\pi-\pi$ stacking. Thereinto, the photocatalytic performance of p-Ag_2S/n-PDI composited photocatalyst was respectively 5.13 times and 1.79 times higher than pure PDI for phenol degradation and O_2 evolution under full-spectrum light irradiation, which indicated the advantage of PDI material. Li [27] et al. studied that a novel $BiVO_4$/self-assembled perylene diimide ($BiVO_4$/PDIsa) organic supermolecule photocatalyst was designed and fabricated via an in situ electrostatic assembling method. The composite material displayed a higher photocatalytic performance for TC degradation, which could reach the degradation efficiency of 81.75% within 30 min under visible light irradiation. The enhanced photocatalytic active was mainly due to the introduction of PDI material. Similarly, PDI as a novel and highly efficient cocatalyst was introduced on graphitic carbon nitride/bismuth tungstate composite to enhance the photocatalytic degradation of tetracycline in water [28]. These results furtherly demonstrate that the PDI material can be considered as an excellent material to improve the photocatalytic performance of semiconductor photocatalyst.

According to the above reasons, a ternary PDI/BiOCl-$BiPO_4$ composited material was designed and prepared. The PDI/BiOCl-$BiPO_4$ composited photocatalysts were evaluated by the degradation of RhB, and the degradation of tetracycline hydrochloride under visible light or simulated solar light irradiation. The PDI/BiOCl-$BiPO_4$ composited photocatalysts were detailedly characterized by X-ray diffraction (XRD), UV-vis diffuse reflectance (UV-vis DRS), Scanning electron microscopy (SEM), and Fourier transform infrared (FTIR) spectroscopies. Obviously, the light absorption capacity of composited material was remarkably enhanced. In addition, the improved photocatalytic activity can be manifested by the photoelectrochemical tools. The photocatalytic reaction process also was demonstrated by the active species trapping experiments. Herein, the possible reaction pathway was proposed via the above results and analysis.

2. Results and Discussion

The crystal structure and composition of PDI, BiOCl, BiOCl-$BiPO_4$ and PDI/BiOCl-$BiPO_4$ composite photocatalysts with the different PDI contents were characterized by X-ray diffraction (XRD) measurement, as shown in Figure 1. The BiOCl-$BiPO_4$ composite material showed the main specific diffractive peaks at 2θ = 12.0°, 24.1°, 25.9°, 32.5°, 33.5°, 36.6°, 40.9°, 46.7°, 49.7°, 54.1°, and 58.6°, which could be assigned to the (001), (002), (101), (110), (102), (003), (112), (200), (113), (211) and (212) lattice planes respectively for the tetragonal phase BiOCl (JCPDS.NO.06-0249). [29] In addition, the diffraction peaks of 2θ appeared in 20.1°, 29.5°, 31.3° could be well indexed to (101), (200), (102) crystal planes of hexagonal phase $BiPO_4$ (JCPDS No. 15-0766) [30], respectively. These results indicated that the BiOCl-$BiPO_4$ composite material was successfully prepared. Furthermore, the diffraction peaks at P0 and P1 were attributed to the characteristic peaks of PDI material, and the XRD diffraction pattern in the range of 24–28° could be ascribed to the π−π stacking structure. It can be easily found that the relative intensity of P1 was higher than that of P0, suggesting that PDI had a highly ordered π−π stacking structure and small d-spacing of π−π stacking after self-assembly [31,32]. The special structure was beneficial to the migration of photogenerated electron-hole pairs, which was convenient for the improvement of photocatalytic performance. Compared to the nude PDI, the PDI/BiOCl-$BiPO_4$ composited material also showed the characteristic diffraction peaks of PDI, revealing that PDI/BiOCl-$BiPO_4$ composited materials were successfully synthesized by the multi-step compound method.

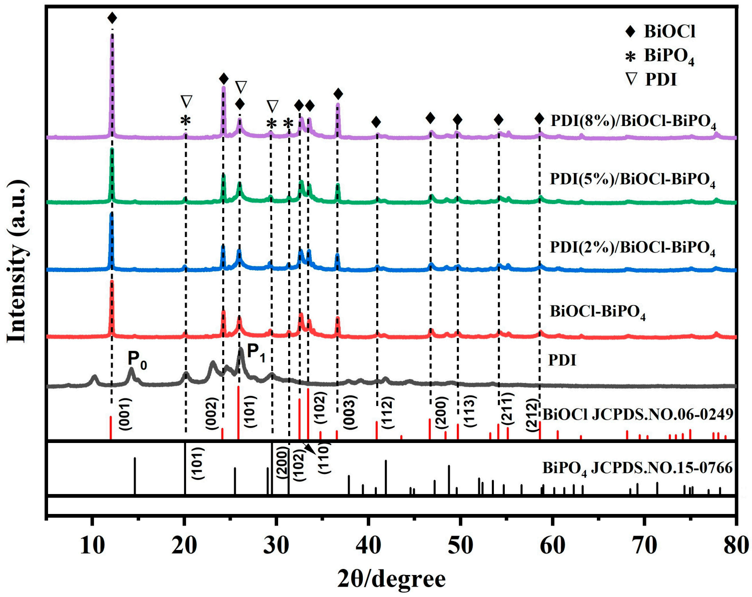

Figure 1. The XRD patterns of PDI, BiOCl-$BiPO_4$, PDI(2%)/BiOCl-$BiPO_4$, PDI(5%)/BiOCl-$BiPO_4$ and PDI(8%)/BiOCl-$BiPO_4$ samples.

The composition of PDI, BiOCl-$BiPO_4$, PDI(2%)/BiOCl-$BiPO_4$, PDI(5%)/BiOCl-$BiPO_4$ and PDI(8%)/BiOCl-$BiPO_4$ samples was furtherly demonstrated by Fourier transformed infrared spectra (FTIR) measurement, as exhibited in Figure 2. For PDI/BiOCl-$BiPO_4$ composite photocatalysts, the characteristic vibration in the range of 1300–600 cm^{-1} was ascribed to the PO_4^{3-} ions, implying the existence of $BiPO_4$ material in the as-prepared BiOCl-$BiPO_4$ and PDI/BiOCl-$BiPO_4$ composited photocatalysts. Thereinto, 1032 cm^{-1} and 598 cm^{-1} were ascribed to the stretching vibration and bending vibration of O-P-O in PO_4 group, respectively [23,30]. Combining with the XRD pattern results, it can be obtained that the $BiPO_4$ is successfully introduced on the BiOCl material to construct the BiOCl-$BiPO_4$, PDI/BiOCl-$BiPO_4$ composite materials. The peaks of PDI supermolecule were mainly focused at 1653 cm^{-1} and 1695 cm^{-1}, which were assigned to C=C and C=O stretching vibrations, respectively [24,31]. Obviously, the PDI/BiOCl-$BiPO_4$ composite photocatalysts with different PDI contents also displayed the weak signal of the typical PDI characteristic peaks, indicating the existence of PDI in the as-prepared composited photocatalyst. The result furtherly uncovers that the PDI/BiOCl-$BiPO_4$ composited materials are successfully synthesized by the multi-step compound method. Furthermore, the SEM images of BiOCl-$BiPO_4$, PDI and PDI(5%)/BiOCl-$BiPO_4$ were shown in Figure 3. Distinctly, Figure 3a,b showed that the BiOCl-$BiPO_4$ sample was composed of some particles and blocks. Figure 3c,d displayed that the PDI material was a layered structure to form the large-block material. After the combination of PDI and BiOCl-$BiPO_4$ materials, their morphologies were reconstructed, as exhibited in Figure 3e,f.

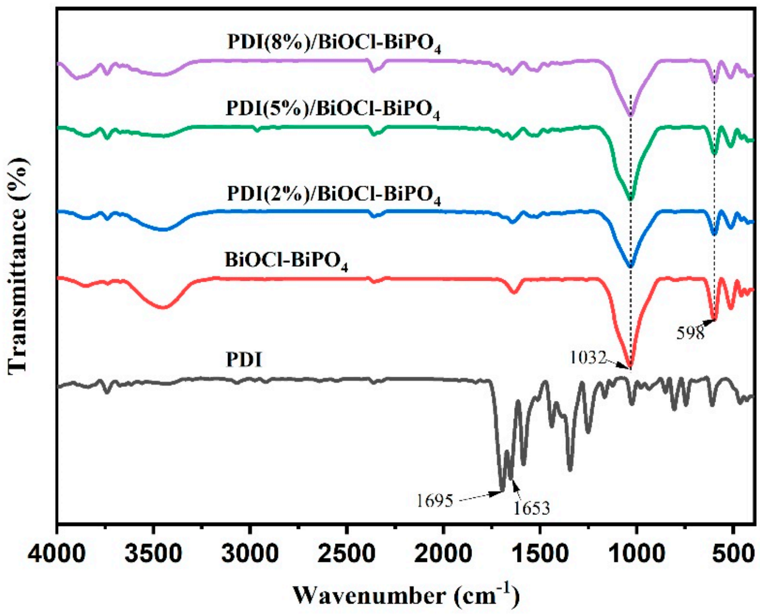

Figure 2. FT-IR spectra of PDI, BiOCl-$BiPO_4$, PDI(2%)/BiOCl-$BiPO_4$, PDI(5%)/BiOCl-$BiPO_4$ and PDI(8%)/BiOCl-$BiPO_4$ samples.

The optical properties of PDI, BiOCl-$BiPO_4$, PDI(2%)/BiOCl-$BiPO_4$, PDI(5%)/BiOCl-$BiPO_4$ and PDI(8%)/BiOCl-$BiPO_4$ samples were researched by UV–vis DRS measurement, as exhibited in Figure 4. Evidently, the BiOCl-$BiPO_4$ composite photocatalyst revealed the light absorption ability in UV light region, indicating that it possesses the UV-light photocatalytic performance. In addition, the DRS pattern of PDI material showed a large range of visible light region, suggesting that it owns the visible light absorption ability. After the incorporation of PDI material on the BiOCl-$BiPO_4$ composite photocatalyst, the visible light absorption ability of BiOCl-$BiPO_4$ composite photocatalyst had a significant enhancement, and their absorption efficiencies were gradually improved with the PDI content increasing, suggesting that the PDI can improve the light absorption ability and range of semiconductor photocatalyst. This phenomenon manifests that the PDI material plays an important role in the composite materials and the enhancement of light absorption ability is beneficial to photocatalytic reaction process.

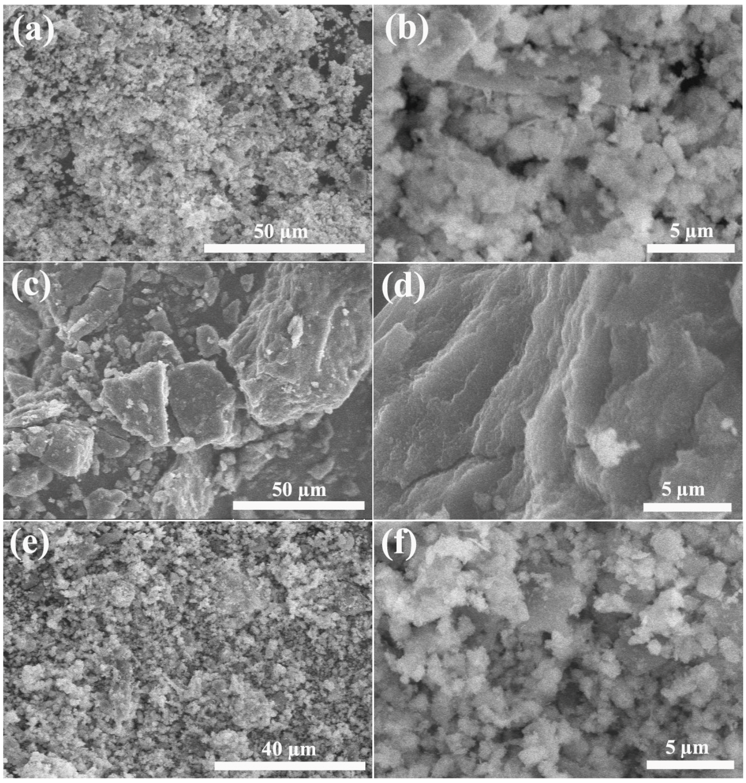

Figure 3. SEM images of BiOCl-$BiPO_4$ (**a**,**b**), PDI (**c**,**d**) and PDI(5%)/BiOCl-$BiPO_4$ (**e**,**f**).

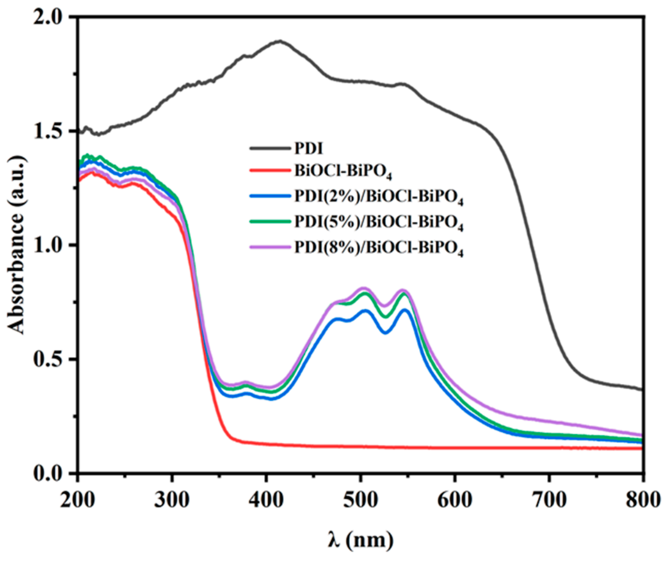

Figure 4. UV-vis DRS spectra of PDI, BiOCl-$BiPO_4$, PDI(2%)/BiOCl-$BiPO_4$, PDI(5%)/BiOCl-$BiPO_4$ and PDI(8%)/BiOCl-$BiPO_4$ samples.

The photocatalytic performance of PDI, BiOCl-$BiPO_4$, PDI(2%)/BiOCl-$BiPO_4$, PDI(5%)/BiOCl-$BiPO_4$ and PDI(8%)/BiOCl-$BiPO_4$ samples was investigated through the degradation of Rhodamine B (RhB) and tetracycline hydrochloride (TCH). Figure 5 showed the photocatalytic activity of RhB degradation for PDI, BiOCl-$BiPO_4$, PDI(2%)/BiOCl-$BiPO_4$, PDI(5%)/BiOCl-$BiPO_4$ and PDI(8%)/BiOCl-$BiPO_4$ samples. Evidently, the blank experiment exhibited a negligible activity, and the nude PDI also displayed a weak photocatalytic performance in comparison to the other composite materials. However, after the incorporation of BiOCl-$BiPO_4$ composited semiconductors, the PDI/BiOCl-$BiPO_4$ composite photocatalysts had an enhancement photocatalytic performance for the degradation of RhB. Thereinto, the degradation efficiencies of PDI(5%)/BiOCl-$BiPO_4$, BiOCl-$BiPO_4$ and PDI samples were 98%, 97% and 79% respectively, as shown in Figure S1. The composite materials showed a close degradation efficiency in 150 min degradation time, but the degradation rate of PDI(5%)/BiOCl-$BiPO_4$ was much higher than that of the other samples, as displayed in Figure S2. The apparent rate constants (k) of the RhB degradation for PDI(5%)/BiOCl-$BiPO_4$, BiOCl-$BiPO_4$ and PDI samples were 0.037 min^{-1}, 0.027 min^{-1} and 0.07 min^{-1}. It can be obtained that the PDI/BiOCl-$BiPO_4$ composited material showed an enhancement photocatalytic performance in comparison to BiOCl-$BiPO_4$ and PDI materials. The result suggests that the introduction of PDI material does boost the photocatalytic performance of semiconductor photocatalysts, which is in accordance with the DRS measurement. Evidently, it can be obtained that the PDI(5%)/BiOCl-$BiPO_4$ exhibited the highest photocatalytic performance than that of the other composite samples. In order to further explore the stability of PDI/BiOCl-$BiPO_4$ composite photocatalysts, the PDI(5%)/BiOCl-$BiPO_4$ sample was continuously investigated, as shown in Figure S3. There appears slight decrease for the RhB degradation efficiency of PDI(5%)/BiOCl-$BiPO_4$ sample after three cycles, suggesting that the PDI(5%)/BiOCl-$BiPO_4$ composite photocatalyst possesses the stability and reusability. At the same time, these photocatalysts were also applied to the degradation of TCH under simulated solar light or visible light irradiation, as shown in Figure 6a,b. Similarly, it can be easily obtained that the PDI(5%)/BiOCl-$BiPO_4$ photocatalyst owned the highest photocatalytic activity under simulated solar light or visible light irradiation. The degradation efficiency of tetracycline hydrochloride degradation for PDI, BiOCl-$BiPO_4$, PDI(2%)/BiOCl-$BiPO_4$, PDI(5%)/BiOCl-$BiPO_4$ and PDI(8%)/BiOCl-$BiPO_4$ samples was shown in Figure S4. Obviously, the degradation efficiencies of PDI(5%)/BiOCl-$BiPO_4$, BiOCl-$BiPO_4$ and PDI samples were 81%, 77% and 60% simulated solar light irradiation, respectively. The plot of $-\ln (C_t/C_0)$ vs. irradiation time for TCH degradation kinetics furtherly demonstrated the enhancement photocatalytic performance of PDI(5%)/BiOCl-$BiPO_4$. The apparent rate constants (k) of the THC degradation for PDI(5%)/BiOCl-$BiPO_4$, BiOCl-$BiPO_4$ and PDI samples were 0.0135 min^{-1}, 0.0127 min^{-1} and 0.0066 min^{-1}, as displayed in Figure S5.This result is consistent with the result of RhB degradation, indicating the advantage of PDI incorporated. In addition, the photocatalytic performance of PDI/BiOCl-$BiPO_4$ composite photocatalysts has an obvious improvement in comparison to BiOCl-$BiPO_4$ sample under visible light irradiation, indicating that the incorporation of PDI is beneficial to the enhancement of photocatalytic activity. The conclusion is in line with the above result for RhB degradation. Because the introduction of PDI can improve the visible light absorption ability of BiOCl-$BiPO_4$ sample, which is also consistent with the DRS measurement. Besides, the comparison of degradation efficiencies of different photocatalysts was exhibited in Table 1, which fully demonstrated the advantages of PDI/BiOCl-$BiPO_4$ composite photocatalysts. These results fully demonstrate the advantages of PDI material and the application potential in the photocatalysis.

Table 1. Comparison of degradation efficiencies of different photocatalysts.

Catalyst	Pollutant	Pollutant Concentration	Amount of Catalyst	Photocatalytic Efficiency	References
$Bi_5CaTi_4FeO_{18}$	MB	1×10^{-5} M, 100 mL	100 mg	~55%, 180 min	[33]
$Bi_{24}O_{31}Cl_{10}$	TCH	10 mg L^{-1}, 100 mL	100 mg	80.1%, 150 min	[34]
Cu_2O–TiO_2	TCH	30 mg L^{-1}, 50 mL	50 mg	81.4%, 240 min	[35]
CdS-TiO_2	TCH	50 mg L^{-1}, 50 mL	50 mg	87%, 480 min	[36]
$Bi_{2.5}Sr_{1.5}Nb_2Ti_{0.5}Cr_{0.5}O_{12}$	TC	6.66 mg L^{-1}, 50 mL	100 mg	89%, 300 min	[37]
PDI(5%)/BiOCl-$BiPO_4$	RhB	10 mg L^{-1}, 50 mL	25 mg	98%, 150 min	Present work
PDI(5%)/BiOCl-$BiPO_4$	TCH	10 mg L^{-1}, 50 mL	25 mg	81%, 150 min	Present work

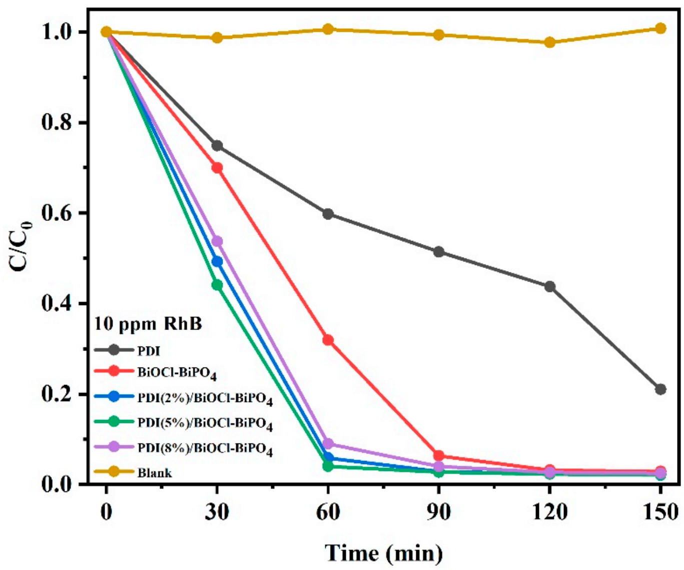

Figure 5. The photocatalytic activity of RhB degradation for all of as-prepared samples as a function of irradiation time under metal halide lamp irradiation.

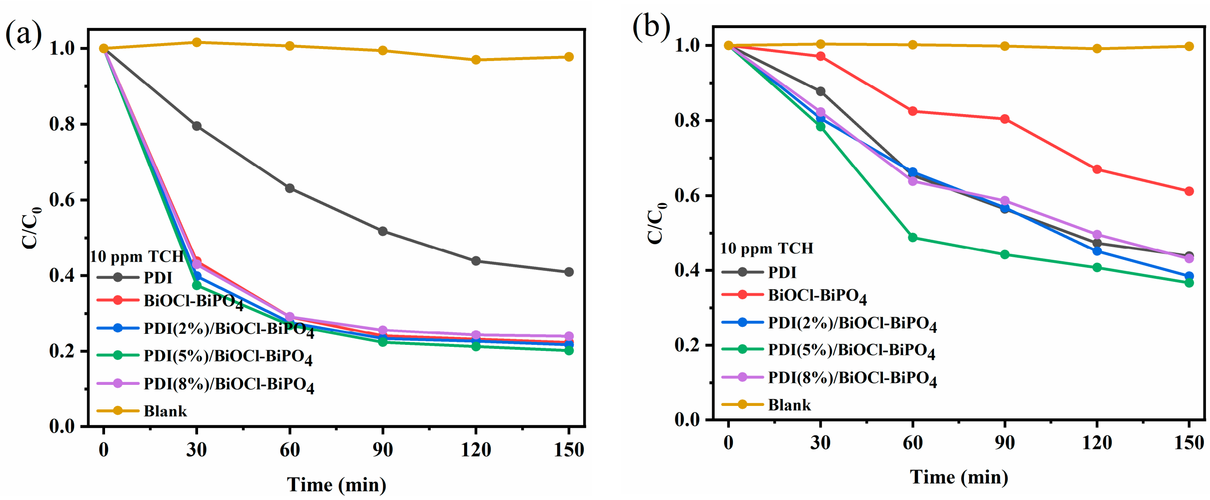

Figure 6. The photocatalytic activity of tetracycline hydrochloride degradation for PDI, BiOCl-$BiPO_4$, PDI(2%)/BiOCl-$BiPO_4$, PDI(5%)/BiOCl-$BiPO_4$ and PDI(8%)/BiOCl-$BiPO_4$ samples as a function of irradiation time (**a**) under simulated solar light irradiation (**b**) under visible light irradiation.

In order to furtherly explore the possible reaction mechanism in photocatalytic reaction process, the active species trapping experiments of PDI(5%)/BiOCl-$BiPO_4$ sample as a model material were carried out, as displayed in Figure 7. Generally speaking, the t-BuOH, EDTA-2Na and p-benzoquinone (BQ) were used as the scavengers to trap hydroxyl radicals (•OH), holes (h^+) and superoxide radicals (•O_2^-), respectively. Prominently, it can be found that no obvious inhibiting action can be found using 1 mmol/L t-BuOH as the scavenger to quench the •OH, but the degradation rate of RhB decreased in a certain extent in this photocatalytic reaction process. This phenomenon illustrates that the •OH is not main active species in the PDI(5%)/BiOCl-$BiPO_4$ system. Interestingly, it can be seen that the degradation efficiency was completely inhibited after the addition of BQ and EDTA-2Na, suggesting that the h^+ and •O_2^- active species played an important role in the PDI/BiOCl-$BiPO_4$ composited photocatalyst in the photocatalytic reaction process. Herein, it can be concluded that the h^+ and •O_2^- were the main active species in the PDI/BiOCl-$BiPO_4$ composited photocatalysts.

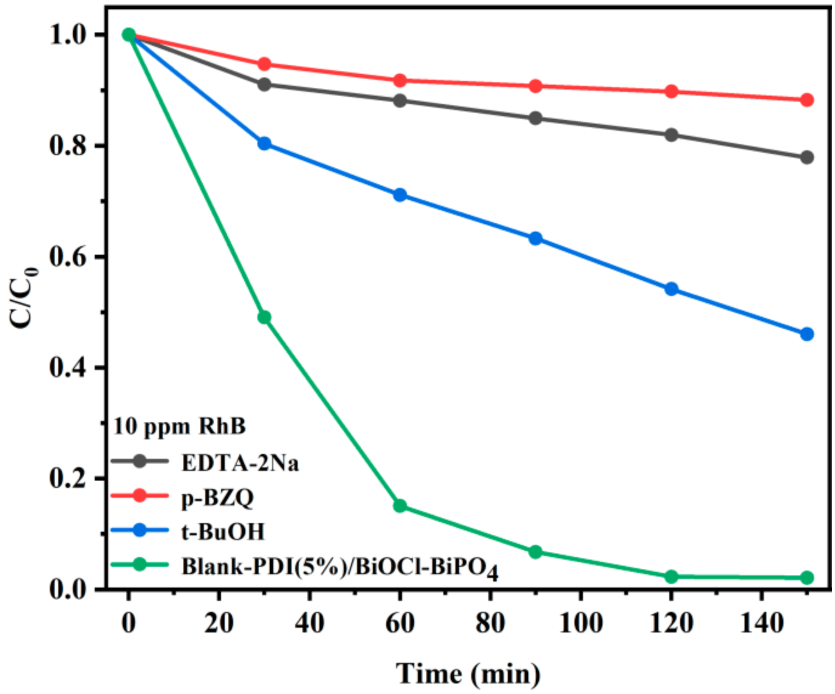

Figure 7. Active species trapping experiment of PDI(5%)/BiOCl-$BiPO_4$ sample in the photocatalytic reaction process.

The migration and separation efficiencies of photo-generated charge carriers can be reflected and monitored by photoelectrochemical (PEC) measurement, as demonstrated in Figure 8. In a general way, the photocurrent intensity can disclose the separation efficiency of photo-generated charge carriers. In addition, an effective charge carrier separation and a fast interfacial charge transfer process can be monitored by the electrochemical impedance spectroscopy (EIS) measurement [38]. Obviously, the PDI/BiOCl-$BiPO_4$ sample displayed the higher photocurrent density than that of the BiOCl-$BiPO_4$ sample, suggesting that PDI/BiOCl-$BiPO_4$ samples possessed a much higher separation efficiency of photo-generated charge carrier. For PDI/BiOCl-$BiPO_4$ samples, the PDI(5%)/BiOCl-$BiPO_4$ sample showed the highest photocurrent density than that of PDI(2%)/BiOCl-$BiPO_4$ and PDI(8%)/BiOCl-$BiPO_4$ samples, indicating that the optimal content of PDI material was 5%. In addition, it can be easily obtained that the above result is consistent with the sequence for photocatalytic performance measurement. In a general way, a stronger transportation ability of charge carriers can be directly reflected by a smaller radius of the semicircle. What is more interesting is that the curve radius on the EIS Nyquist plot of PDI(5%)/BiOCl-$BiPO_4$ sample is smaller than that of the other samples, indicating that the improved charge carrier separation and charge carrier mobility is in line with the above photocurrent pattern. In addition, the results can be furtherly demonstrated by the PL measurement, as shown in Figure 9. The photoluminescence (PL) emission spectra have been widely used to investigate the efficiency of charge carrier trapping, migration and transfer, and understand the fate of electron/hole pairs in semiconductor particles. The lower PL intensity of PDI(5%)/BiOCl-$BiPO_4$ sample indicated that it possessed the weaker recombination probability of photo-generated electron-hole pairs. These results demonstrate that the introduction of PDI can reduce the recombination of photo-generated holes and electrons and be beneficial to the photocatalytic reaction process.

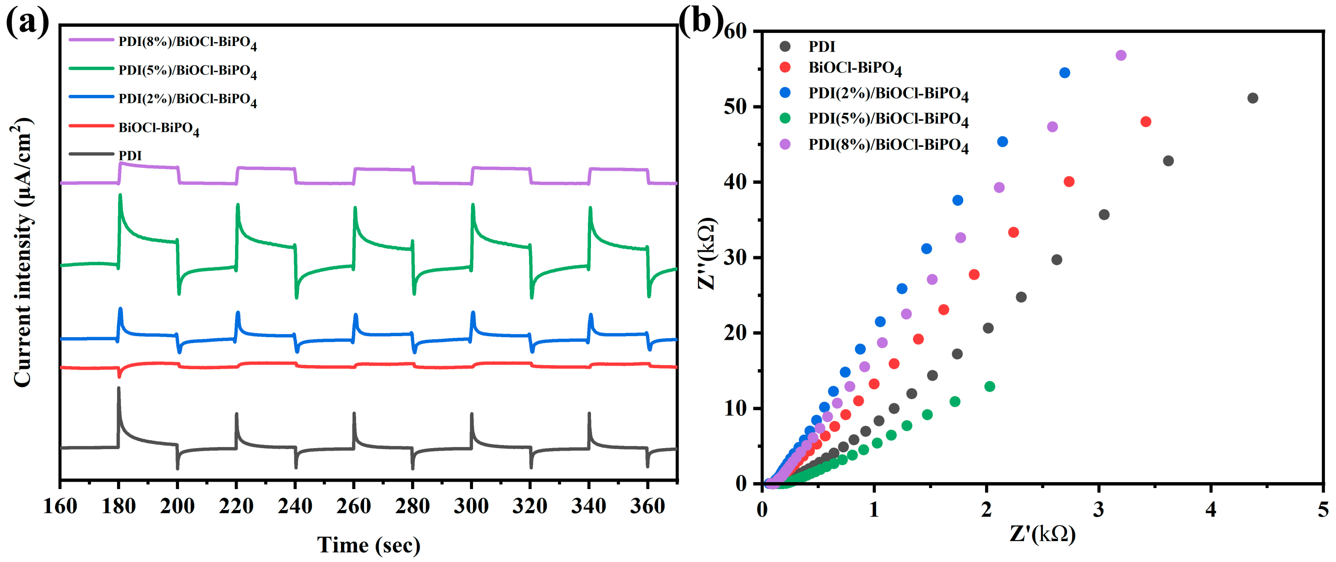

Figure 8. (**a**) The transient photocurrent response of PDI, BiOCl-$BiPO_4$, PDI(2%)/BiOCl-$BiPO_4$, PDI(5%)/BiOCl-$BiPO_4$ and PDI(8%)/BiOCl-$BiPO_4$ samples simulated solar light irradiation. (**b**) The electrochemical impedance spectroscopy (EIS) of PDI, BiOCl-$BiPO_4$, PDI(2%)/BiOCl-$BiPO_4$, PDI(5%)/BiOCl-$BiPO_4$ and PDI(8%)/BiOCl-$BiPO_4$ samples.

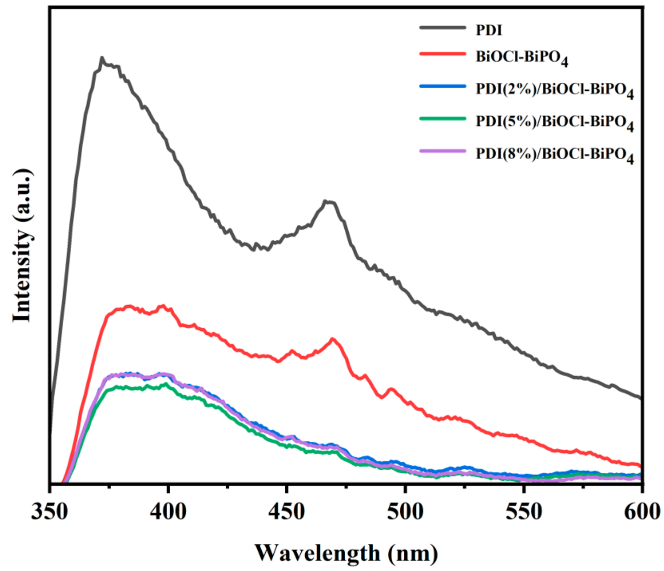

Figure 9. Steady-state fluorescence spectra of PDI, BiOCl-$BiPO_4$, PDI(2%)/BiOCl-$BiPO_4$, PDI(5%)/BiOCl-$BiPO_4$ and PDI(8%)/BiOCl-$BiPO_4$ samples.

Based on the above experimental results and previous reports, a possible photocatalytic reaction mechanism is proposed. The possible mechanism of the enhanced photocatalytic activity for composite PDI/BiOCl-$BiPO_4$ photocatalyst is shown in Figure 10. Firstly, the PDI and BiOCl-$BiPO_4$ materials were irradiated under simulated solar light, and the photo-generated electrons and holes will be produced in the conductor band (CB) and valence band (VB) position of material. Because of the existence of p-n heterostructure between BiOCl and $BiPO_4$ materials [39,40], the photo-generated electrons will migrate toward $BiPO_4$. Besides, it can be obtained from the previous reports that the E_{CB} and E_{VB} for BiOCl ($BiPO_4$) were −0.43 and 3.02 eV (−0.34 and 3.53 eV for $BiPO_4$) respectively [41], and the E_{CB} and E_{VB} of PDI were −0.93 and 0.87 eV [42]. If the separation and transfer pathway of photo-generated electron-hole pairs follows the type II heterojunction, the electrons in the CB position of PDI will be transferred to the CB position of BiOCl-$BiPO_4$ and holes in the VB position of BiOCl-BiPO$_4$ will be transferred to VB position of PDI. However, when the holes of VB position of BiOCl-BiPO$_4$ were transferred to the VB position of PDI, it did not have enough ability to oxidize H_2O into the •OH radicals ($E_{\bullet OH/H2O}$ = +2.68 V vs. NHE) [43], because it owned more negative potential. Therefore, when the PDI and BiOCl/BiPO$_4$ materials are irradiated, the photo-generated electrons and holes maybe follow the Z-scheme transfer mechanism to accomplish the photocatalytic reaction.

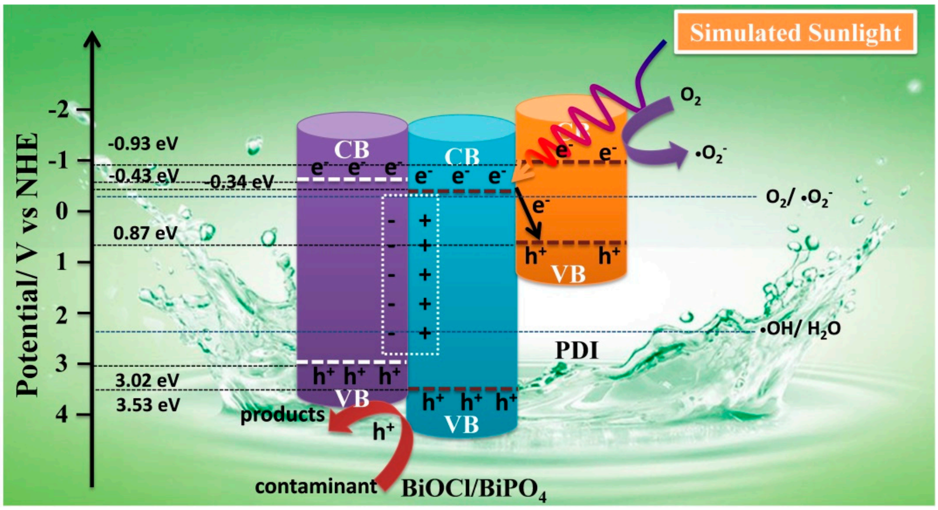

Figure 10. Proposed mechanism of the enhanced photocatalytic activity for PDI/BiOCl-BiPO$_4$ composite photocatalysts.

3. Experimental Section

3.1. Experimental Materials

All the chemicals involving in synthetic catalysts were of analytical reagent grade and no further purification. Bismuth nitrate pentahydrate ($Bi(NO_3)_3 \cdot 5H_2O$), sodium phosphate dibasic dodecahydrate ($NaH_2PO_4 \cdot 12H_2O$), hexamethylene tetramine ($C_6H_{12}N_4$), potassium chloride (KCl), lithiumchloride (LiCl), perylene-3,4,9,10-tetracarboxylic dianhydride (PTCD), imidazole ($C_3H_4N_2$), 3-aminopro-pionic acid ($C_3H_7NO_2$) trimethylamine ($C_6H_{15}N$), hydrochloric acid (HCl), nitric acid (HNO_3), ethanol (EtOH), rhodamine B (RhB), tetracycline hydrochloride (TCH) benzoquinone (BQ), tert-butyl alcohol (t-BuOH), ethylenediaminetetraacetic acid disodium (EDTA-2Na). Deionized water was used for all the experiments.

3.2. Catalyst Preparation

PDI: Firstly, 1.38 g (3.507 mM) of perylene-3, 4, 9, 10-tetracarboxylic dianhydride, 18 g of imidazole and 2.50 g (28.06 mM) of 3-aminopro-pionic acid were heated at 110 °C for 4 h under the protection of argon in a three–necked flask. In the next moment, the reaction mixture was dispersed in 300 mL of HCl (2 M) and 100 mL ethanol, and they were continuously stirred for one night. Then, the final red solid was washed to neutral with distilled water and filtrated through a 0.22 µm membrane filter. Finally, the collected red solid was dried under vacuum at 60 °C in oven and powdered for further applications.

0.54 g of bulk PDI was dispersed in deionized water (100 mL). Then, triethylamine (800 µL) was added under vigorous stirring. After stirring for 1 h, nitric acid (4.0 M, 35 mL) was added and then the mixture was stirred again for 3 h to form the self-assembled PDI as a dark red solid, which was fully washed and centrifuged. Finally, the collected sample was placed in a vacuum drier at 60 °C.

BiOCl-BiPO$_4$: In a typical procedure, 5.0 g of $Bi(NO_3)_3 \cdot 5H_2O$ was dispersed on 15 mL deionized water in a three–necked flask, then 5.5 mL of concentrated HNO_3 was added into the above solution and continuously stirred until the reaction mixture was dissolved. In the next moment, 3.0 g of hexamethylene tetramine was dissolved in 15 mL of deionized water and transferred into the above reaction solution, and 5 mL of deionized water was used to wash the remaining sample. Subsequently, the three–necked flask were heated and kept reflux reaction at 80 °C for 6 h. The obtained $Bi(OH)_3$ sample was further dried at 60 °C after reaction. The $Bi(OH)_3$, KCl, LiCl and NaH_2PO_4 samples (mass ratio $Bi(OH)_3$:KCl:LiCl = 0.6:3.3:2.7 and molar ratio $Bi(OH)_3$:KCl:LiCl = 0.6:3.3:2.7) were mixed and fully grinded. Next, these samples were transferred into a crucible at 500 °C for 2 h. Finally, the collected sample was dispersed in deionized water, and was washed and filtrated, and the collected sample was placed in a vacuum drier at 60 °C.

PDI/BiOCl-$BiPO_4$: The PDI samples with different qualities and 0.5 g of BiOCl-$BiPO_4$ sample were dispersed in 50 mL of ethanol in a 100 mL Teflon autoclave, and these samples were uniformly mixed by ultrasonication for 60 min. In the next moment, the mixed solution was sealed and maintained at 150 °C for 4 h. Finally, the sample was washed to neutral with distilled water and filtrated through a 0.22 μm membrane filter, and it was dried under vacuum at 60 °C in oven. The mass contents of PDI in the PDI/BiOCl-$BiPO_4$ composite materials were adjusted to be 2%, 5% and 8%, which were labeled as PDI(2%)/BiOCl-$BiPO_4$, PDI(5%)/BiOCl-$BiPO_4$ and PDI(8%)/BiOCl-$BiPO_4$, respectively.

3.3. Characterization of Samples

The morphological features were tested through scanning electron microscopy (SEM) using a field emission scanning electron microscope (SU8000). Bruker D8 Advance X-ray diffractometer was operated for testing the X-ray diffraction (XRD) patterns of samples with Cu Kα radiation (λ = 0.15406 nm) at 40 kV and 40 mA. UV–Vis diffuse reflectance spectra (DRS) were measured by UV–Vis spectrophotometer (UV-2600, Shimadzu, Kyoto, Japan), in which BaSO4 powder was took as the internal reflectance sample to collect the optical properties over a wavelength range of 200–800 nm. Photoluminescence (PL) spectra were analyzed by FLS980 fluorescence spectrometer at the excitation wavelength of λ = 320 nm. The Fourier transformed infrared spectra (FTIR) were in measurements on a Nicolet 4700 FT-IR spectrometer by KBr pellets. The photoelectrochemical measurements including the photocurrent test, impedance spectra (EIS), and Mott−Schottky (MS) were detected in an electrochemical workstation (CHI660E, Shanghai, China) coupled with a traditional three electrode cell, in which Ag/AgCl electrode was performed as the reference electrode and platinum wires was as the counter electrode. Overall, 10 mg of the sample was dispersed in three drops of ethanol including 10 μL of Nafion solution, and then the solution was under ultrasonication for 40 min. Herein, Ag/AgCl was used as a reference counter, a Pt wire were used as a counter electrode, and an indium tin oxide (ITO) conducting glass dropped by samples was used as a working electrode. The electrolyte solution (pH = 7.56) was 0.1 M Na_2SO_4. The photocurrent tests were carried out under the visible light illumination.

3.4. Photocatalytic Activity Measurement

Photocatalytic performances for tetracycline hydrochloride (TCH) and Rhodamine B (RhB) were investigated under the simulated solar light or visible light irradiation. The detailed process was carried out as follows. Before exposure to light, 25 mg of photocatalyst was added into 50 mL of 10 mg/L pollutant aqueous solution in a container. Prior to irradiation, the suspensions were magnetically stirred in dark for 40 min to ensure the establishment of an adsorption/desorption equilibrium between the photocatalyst and pollutant. At given irradiation time intervals, 3–4 mL of suspension was collected and centrifuged to remove the photocatalyst particles, then the residual pollutant solution was analyzed by monitoring variations at the wavelength of maximal absorption in the UV-vis spectra (UV-6300 spectrophotometer).

In order to probe the active species generated in the photocatalytic reaction process, the t-BuOH, EDTA-2Na and p-benzoquinone (BQ) as the scavengers of hydroxyl radicals (•OH), holes (h^+)and superoxide radicals (•O_2^-) were respectively added into the RhB solution to study the influence of different active species. The concentrations of t-BuOH, EDTA-2Na and BQ were 1 mmol/L. The photocatalytic degradation reaction was similar to the above test condition except for adding scavengers in the RhB solution.

4. Conclusions

In this work, a ternary PDI/BiOCl-$BiPO_4$ composited material with the different contents of PDI material was designed and prepared by the multi-step compound method. The structure and component could be confirmed by the XRD and IR tools. The PDI/BiOCl-$BiPO_4$ composite photocatalyst presented the improved absorption ability in comparison to the BiOCl-$BiPO_4$ sample. The optimized PDI/BiOCl-$BiPO_4$ photocatalyst, namely PDI(5%)/BiOCl-$BiPO_4$ sample, has the highest photocatalytic degradation performance. It is found that the h^+ and $\bullet O_2^-$ are major active species by the active species trapping experiments. The PEC and PL characterizations demonstrate that the incorporation of PDI material markedly reinforces the separation and transfer efficiency of photo-excited electron-hole pairs, and prolong its life time in PDI(5%)/BiOCl-$BiPO_4$ sample. In addition, a possible reaction mechanism that the ternary PDI/BiOCl-$BiPO_4$ composited materials maybe follow the Z−Scheme reaction mechanism to participate in the photocatalytic reaction process was proposed. This work provides an effective strategy to construct the efficient composite photocatalyst for contaminant degradation.

Supplementary Materials: The following supporting information can be downloaded at: https://www.mdpi.com/article/10.3390/catal13040688/s1, Figure S1: The degradation efficiency of all of as-prepared samples for RhB degradation; Figure S2: Plot of -ln (C_t/C_0) vs. irradiation time shows RhB degradation kinetics; Figure S3: Stability test of PDI(5%)/BiOCl-BiPO4 sample for RhB degradation; Figure S4: The degradation efficiency of tetracycline hydrochloride degradation for PDI, BiOCl-$BiPO_4$, PDI(2%)/BiOCl-$BiPO_4$, PDI(5%)/BiOCl-$BiPO_4$ and PDI(8%)/BiOCl-$BiPO_4$ samples under simulated solar light irradiation; Figure S5: Plot of -ln (C_t/C_0) vs. irradiation time shows TCH degradation kinetics under simulated solar light irradiation.

Author Contributions: H.Z.: Writing—original draft, Supervision. F.W.: Methodology. K.S.: Resources. K.Y.: Supervision. All authors have read and agreed to the published version of the manuscript.

Funding: We are grateful for financial support from National Natural Science Foundation of China (21962006), Jiangxi Provincial Academic and Technical Leaders Training Program–Young Talents (20204BCJL23037), Program of Qingjiang Excellent Young Talents, JXUST (JXUSTQJBJ2020005), Ganzhou Young Talents Program of Jiangxi Province (204301000111), Postdoctoral Research Projects of Jiangxi Province in 2020 (204302600031), Jiangxi Province "Double Thousand Plan" (Yang Kai), Natural Science Foundation of Fujian Province for Youths (Grant No. 2021J05180).

Data Availability Statement: The original contributions presented in the study are included in the article; further inquiries can be directed to the corresponding author.

Conflicts of Interest: The authors declare no conflict of interest.

References

1. Wu, C.-J.; Valerie Maggay, I.; Chiang, C.-H.; Chen, W.; Chang, Y.; Hu, C.; Venault, A. Removal of tetracycline by a photocatalytic membrane reactor with MIL-53(Fe)/PVDF mixed-matrix membrane. *Chem. Eng. J.* **2023**, *451*, 138990. [CrossRef]
2. Guo, F.; Huang, X.; Chen, Z.; Sun, H.; Shi, W. Investigation of visible-light-driven photocatalytic tetracycline degradation via carbon dots modified porous $ZnSnO_3$ cubes: Mechanism and degradation pathway. *Sep. Purif. Technol.* **2020**, *253*, 117518. [CrossRef]
3. Jiang, H.; Wang, Q.; Chen, P.; Zheng, H.; Shi, J.; Shu, H.; Liu, Y. Photocatalytic degradation of tetracycline by using a regenerable (Bi)BiOBr/rGO composite. *J. Clean. Prod.* **2022**, *339*, 130771. [CrossRef]
4. Olusegun, S.J.; Larrea, G.; Osial, M.; Jackowska, K.; Krysinski, P. Photocatalytic Degradation of Antibiotics by Superparamagnetic Iron Oxide Nanoparticles. Tetracycline Case. *Catalysts* **2021**, *11*, 1243. [CrossRef]
5. He, Z.; Siddique, M.S.; Yang, H.; Xia, Y.; Su, J.; Tang, B.; Wang, L.; Kang, L.; Huang, Z. Novel Z-scheme In_2S_3/Bi_2WO_6 core-shell heterojunctions with synergistic enhanced photocatalytic degradation of tetracycline hydrochloride. *J. Clean. Prod.* **2022**, *339*, 130634. [CrossRef]
6. Cheng, M.; Zhang, Y.; Lai, B.; Wang, L.; Yang, S.; Li, K.; Wang, D.; Wu, Y.; Chen, G.-H.; Qian, J. Nitrogen and phosphorus co-doped porous carbons (NPCs) for peroxydisulfate (PDS) activation towards tetracycline degradation: Defects enhanced adsorption and non-radical mechanism dominated by electron transfer. *Chem. Eng. J.* **2022**, *455*, 140615. [CrossRef]

7. Chen, W.; Huang, J.; He, Z.-C.; Ji, X.; Zhang, Y.-F.; Sun, H.-L.; Wang, K.; Su, Z.-W. Accelerated photocatalytic degradation of tetracycline hydrochloride over $CuAl_2O_4/g\text{-}C_3N_4$ p-n heterojunctions under visible light irradiation. *Sep. Purif. Technol.* **2021**, *277*, 119461. [CrossRef]
8. Pei, C.-Y.; Chen, Y.-G.; Wang, L.; Chen, W.; Huang, G.-B. Step-scheme $WO_3/CdIn_2S_4$ hybrid system with high visible light activity for tetracycline hydrochloride photodegradation. *Appl. Surf. Sci.* **2021**, *535*, 147682. [CrossRef]
9. Liu, S.-y.; Zada, A.; Yu, X.; Liu, F.; Jin, G. $NiFe_2O_4/g\text{-}C_3N_4$ heterostructure with an enhanced ability for photocatalytic degradation of tetracycline hydrochloride and antibacterial performance. *Chemosphere* **2022**, *307*, 135717. [CrossRef]
10. Zhang, X.-W.; Wang, F.; Wang, C.-C.; Wang, P.; Fu, H.; Zhao, C. Photocatalysis activation of peroxodisulfate over the supported Fe_3O_4 catalyst derived from MIL-88A(Fe) for efficient tetracycline hydrochloride degradation. *Chem. Eng. J.* **2021**, *426*, 131927. [CrossRef]
11. Abdullah, F.H.; Bakar, N.H.H.A.; Bakar, M.A. Current advancements on the fabrication, modification, and industrial application of zinc oxide as photocatalyst in the removal of organic and inorganic contaminants in aquatic systems. *J. Hazard. Mater.* **2022**, *424*, 127416. [CrossRef] [PubMed]
12. Liu, X.; Zhuang, H. Recent progresses in photocatalytic hydrogen production: Design and construction of Ni-based cocatalysts. *Int. J. Energy Res.* **2021**, *45*, 1480–1495. [CrossRef]
13. Zhuang, H.; Chen, X.; Xia, J.; Lu, K.; Huang, W.; Liu, X.; Yu, C.; Yang, K. State-of-the-art progress in Ag_3PO_4-based photocatalysts: Rational design, regulation and perspective. *Appl. Mater. Today* **2023**, *31*, 101742. [CrossRef]
14. Raja, A.; Son, N.; Pandey, S.; Kang, M. Fabrication of solar-driven hierarchical $ZnIn_2S_4/rGO/SnS_2$ heterojunction photocatalyst for hydrogen generation and environmental pollutant elimination. *Sep. Purif. Technol.* **2022**, *293*, 121119. [CrossRef]
15. Ouyang, C.; Quan, X.; Zhang, C.; Pan, Y.; Li, X.; Hong, Z.; Zhi, M. Direct Z-scheme $ZnIn_2S_4@MoO_3$ heterojunction for efficient photodegradation of tetracycline hydrochloride under visible light irradiation. *Chem. Eng. J.* **2021**, *424*, 130510. [CrossRef]
16. Sun, L.; Xiang, L.; Zhao, X.; Jia, C.-J.; Yang, J.; Jin, Z.; Cheng, X.; Fan, W. Enhanced visible-light photocatalytic activity of BiOI/BiOCl heterojunctions: Key role of crystal facet combination. *ACS Catal.* **2015**, *5*, 3540–3551. [CrossRef]
17. Zhuang, H.; Huang, Y.; Lin, l.; Xu, W.; Liu, X. Fabrication of BiOCl nanosheets with oxygen vacancies via a novel strategy for enhanced photocatalytic degradation of rhodamine B. *Mater. Lett.* **2022**, *324*, 132623. [CrossRef]
18. Su, X.; Yang, J.; Yu, X.; Zhu, Y.; Zhang, Y. In situ grown hierarchical 50%BiOCl/BiOI hollow flowerlike microspheres on reduced graphene oxide nanosheets for enhanced visible-light photocatalytic degradation of rhodamine B. *Appl. Surf. Sci.* **2018**, *433*, 502–512. [CrossRef]
19. Zhu, X.; Wang, Y.; Guo, Y.; Wan, J.; Yan, Y.; Zhou, Y.; Sun, C. Environmental-friendly synthesis of heterojunction photocatalysts $g\text{-}C_3N_4/BiPO_4$ with enhanced photocatalytic performance. *Appl. Surf. Sci.* **2021**, *544*, 148872. [CrossRef]
20. Wang, Y.; Qiang, Z.; Zhu, W.; Yao, W.; Tang, S.; Yang, Z.; Wang, J.; Duan, J.; Ma, C.; Tan, R. $BiPO_4$ Nanorod/Graphene Composite heterojunctions for photocatalytic degradation of tetracycline hydrochloride. *ACS Appl. Nano Mater.* **2021**, *4*, 8680–8689. [CrossRef]
21. Mahendran, N.; Praveen, K. $BiPO_4$/Fe-metal organic framework composite: A promising photocatalyst toward the abatement of tetracycline hydrochloride, Indigo Carmine and reduction of 4-nitrophenol. *J. Ind. Eng. Chem.* **2021**, *100*, 220–232. [CrossRef]
22. Wang, Y.-J.; Zhang, J.-Y.; Hou, S.-S.; Wu, J.-X.; Wang, C.; Li, Y.-M.; Jiang, G.-Y.; Cui, G.-Q. Novel CoAl-LDH Nanosheets/$BiPO_4$ nanorods composites for boosting photocatalytic degradation of phenol. *Petrol. Sci.* **2022**, *19*, 3080–3087. [CrossRef]
23. Yang, W.; Tang, S.; Wei, Z.; Chen, X.; Ma, C.; Duan, J.; Tan, R. Separate-free $BiPO_4$/graphene aerogel with 3D network structure for efficient photocatalytic mineralization by adsorption enrichment and photocatalytic degradation. *Chem. Eng. J.* **2021**, *421*, 129720. [CrossRef]
24. Cai, T.; Zeng, W.; Liu, Y.; Wang, L.; Dong, W.; Chen, H.; Xia, X. A promising inorganic-organic Z-scheme photocatalyst Ag_3PO_4/PDI supermolecule with enhanced photoactivity and photostability for environmental remediation. *Appl. Catal. B Environ.* **2020**, *263*, 118327. [CrossRef]
25. Ben, H.; Liu, Y.; Liu, X.; Liu, X.; Ling, C.; Liang, C.; Zhang, L. Diffusion-controlled Z-scheme-steered charge separation across PDI/BiOI heterointerface for ultraviolet, visible, and infrared light-driven photocatalysis. *Adv. Funct. Mater.* **2021**, *31*, 2102315. [CrossRef]
26. Yang, J.; Miao, H.; Li, W.; Li, H.; Zhu, Y. Designed synthesis of a p-Ag_2S/n-PDI self-assembled supramolecular heterojunction for enhanced full-spectrum photocatalytic activity. *J. Mater. Chem. A* **2019**, *7*, 6482–6490. [CrossRef]
27. Li, B.; Chen, S.; Huang, D.; Cheng, M.; Du, C.; Feng, C.; Yang, Y.; Lei, L.; Chen, Y.; Xue, W.; et al. PDI supermolecule-encapsulated 3D $BiVO_4$ toward unobstructed interfacial charge transfer for enhanced visible-light photocatalytic activity. *J. Phys. Chem. C* **2021**, *125*, 18693–18707. [CrossRef]
28. Zhou, W.; Yang, B.; Liu, G.; Xu, C.; Ji, Q.; Xiang, W.; Sun, D.; Zhong, Q.; He, H.; Yazi, L.; et al. Perylene diimide supermolecule (PDI) as a novel and highly efficient cocatalyst for photocatalytic degradation of tetracycline in water: A case study of PDI decorated graphitic carbon nitride/bismuth tungstate composite. *J. Colloid. Interf. Sci.* **2022**, *615*, 849–864. [CrossRef]
29. Hong, W.; Wang, L.; Liu, K.; Han, X.; Zhou, Y.; Gao, P.; Ding, R.; Liu, E. Asymmetric supercapacitor constructed by self-assembled camellia-like BiOCl and activated carbon microspheres derived from sweet potato starch. *J. Alloy. Compd.* **2018**, *746*, 292–300. [CrossRef]
30. Maisang, W.; Phuruangrat, A.; Randorn, C.; Kungwankunakorn, S.; Thongtem, S.; Wiranwetchayan, O.; Wannapop, S.; Choopun, S.; Kaowphong, S.; Thongtem, T. Enhanced photocatalytic performance of visible-light-driven BiOBr/$BiPO_4$ composites. *Mat. Sci. Semicon. Proc.* **2018**, *75*, 319–326. [CrossRef]

31. Wang, J.; Shi, W.; Liu, D.; Zhang, Z.; Zhu, Y.; Wang, D. Supramolecular organic nanofibers with highly efficient and stable visible light photooxidation performance. *Appl. Catal. B Environ.* **2017**, *202*, 289–297. [CrossRef]
32. Datar, A.; Balakrishnan, K.; Zang, L. One-dimensional self-assembly of a water soluble perylene diimide molecule by pH triggered hydrogelation. *Chem. Commun.* **2013**, *49*, 6894–6896. [CrossRef] [PubMed]
33. Naresh, G.; Malik, J.; Meena, V.; Mandal, T.K. pH-mediated collective and selective solar photocatalysis by a series of layered aurivillius perovskites. *ACS Omega* **2018**, *3*, 11104–11116. [CrossRef] [PubMed]
34. Yin, B.; Fang, Z.; Luo, B.; Zhang, G.; Shi, W. Facile Preparation of $Bi_{24}O_{31}Cl_{10}$ Nanosheets for Visible-Light-Driven Photocatalytic Degradation of Tetracycline Hydrochloride. *Catal. Lett.* **2017**, *147*, 2167–2172. [CrossRef]
35. Shi, Y.; Yang, Z.; Wang, B.; An, H.; Chen, Z.; Cui, H. Adsorption and photocatalytic degradation of tetracycline hydrochloride using a palygorskite-supported Cu_2O–TiO_2 composite. *Appl. Clay Sci.* **2016**, *119*, 311–320. [CrossRef]
36. Li, W.; Ding, H.; Ji, H.; Dai, W.; Guo, J.; Du, G. Photocatalytic degradation of tetracycline hydrochloride via a CdS-TiO_2 heterostructure composite under visible light irradiation. *Nanomaterials* **2018**, *8*, 415. [CrossRef]
37. Malik, J.; Kumar, S.; Mandal, T.K. Reactive species specific RhB assisted collective photocatalytic degradation of tetracycline antibiotics with triple-layer Aurivillius perovskites. *Catal. Sci. Technol.* **2022**, *12*, 6704–6716. [CrossRef]
38. Liu, X.; Xu, W.; Wang, N.; Lin, L.; Zhuang, H.; Li, Q. An ultra-high performance for reduction of 4-nitroaniline with optimized noble-metal-free Bi_4NbO_8Cl nanosheets under visible light irradiation. *Adv. Powder Technol.* **2022**, *33*, 103601. [CrossRef]
39. Hu, Y.; Jia, Z.; Lv, R.; Fan, C.; Zhang, H. One-pot electrochemical preparation of BiOCl/$BiPO_4$ double-layer heterojunction film with efficient photocatalytic performance. *Mater. Res. Bull.* **2017**, *94*, 222–230. [CrossRef]
40. Duo, F.; Wang, Y.; Mao, X.; Zhang, X.; Wang, Y.; Fan, C. A $BiPO_4$/BiOCl heterojunction photocatalyst with enhanced electron-hole separation and excellent photocatalytic performance. *Appl. Surf. Sci.* **2015**, *340*, 35–42. [CrossRef]
41. Mei, J.; Tao, Y.; Gao, C.; Zhu, Q.; Zhang, H.; Yu, J.; Fang, Z.; Xu, H.; Wang, Y.; Li, G. Photo-induced dye-sensitized $BiPO_4$/BiOCl system for stably treating persistent organic pollutants. *Appl. Catal. B: Environ.* **2021**, *285*, 119841. [CrossRef]
42. Ji, X.; Liu, X.; Guo, Y.; Zhang, J. Developing visible light responsive Z-scheme BN-PDI photocatalysts with good degradation performance for antibiotics. *Chem. Eng. J.* **2021**, *425*, 131260. [CrossRef]
43. Malik, J.; Kumar, S.; Srivastava, P.; Bag, M.; Mandal, T.K. Cation disorder and octahedral distortion control of internal electric field, band bending and carrier lifetime in Aurivillius perovskite solid solutions for enhanced photocatalytic activity. *Mater. Adv.* **2021**, *2*, 4832–4842. [CrossRef]